Journal of Physics D: Applied Physics

PAPER

Epitaxial (110)-oriented $La_{0.7}Sr_{0.3}MnO_3$ film directly on flexible mica substrate

To cite this article: Lianxu Ye *et al* 2022 *J. Phys. D: Appl. Phys.* **55** 224002

IOP Publishing Journal of Physics D: Applied Physics

J. Phys. D: Appl. Phys. **55** (2022) 224002 (7pp) https://doi.org/10.1088/1361-6463/ac570d

Epitaxial (110)-oriented $La_{0.7}Sr_{0.3}MnO_3$ film directly on flexible mica substrate

Lianxu Ye[1,2], Di Zhang[3], Juanjuan Lu[3], Sicheng Xu[4], Ruixing Xu[1,2], Jiyu Fan[1,2,*], Rujun Tang[4], Haiyan Wang[3], Haizhong Guo[5], Weiwei Li[1,2,*] and Hao Yang[1,2,*]

[1] College of Science, Nanjing University of Aeronautics and Astronautics, Nanjing 211106, People's Republic of China
[2] MIIT Key Laboratory of Aerospace Information Materials and Physics (NUAA), Nanjing 211106, People's Republic of China
[3] School of Materials Engineering and School of Electrical and Computer Engineering, Purdue University, West Lafayette, IN 47907, United States of America
[4] Jiangsu Key Laboratory of Thin Films, School of Physical Science and Technology, Soochow University, Suzhou 215006, People's Republic of China
[5] Key Laboratory of Material Physics, Ministry of Education, School of Physics and Microelectronics, Zhengzhou University, Zhengzhou 450052, People's Republic of China

E-mail: jiyufan@nuaa.edu.cn, wl337@nuaa.edu.cn and yanghao@nuaa.edu.cn

Received 4 October 2021, revised 4 February 2022
Accepted for publication 21 February 2022
Published 4 March 2022

Abstract

Manufacture and characterizations of perovskite-mica van der Waals epitaxy heterostructures are a critical step to realize the application of flexible devices. However, the fabrication and investigation of the van der Waals epitaxy architectures grown on mica substrates are mainly limited to (111)-oriented perovskite functional oxide thin films up to now and buffer layers are highly needed. In this work, we directly grew $La_{0.7}Sr_{0.3}MnO_3$ (LSMO) thin films on mica substrates without using any buffer layer. By the characterizations of x-ray diffractometer and scanning transmission electron microscopy, we demonstrate the epitaxial growth of the (110)-oriented LSMO thin film on the mica substrate. The LSMO thin film grown on the mica substrate via van der Waals epitaxy adopts domain matching epitaxy instead of conventional lattice matching epitaxy. Two kinds of domain matching relationships between the LSMO thin film and mica substrate are sketched by Visualization for Electronic and STructural Analysis software and discussed. A decent ferromagnetism retains in the (110)-oriented LSMO thin film. Our work demonstrates a new pathway to fabricate (110)-oriented functional oxide thin films on flexible mica substrates directly.

Keywords: flexible oxide heterostructures, $La_{0.7}Sr_{0.3}MnO_3$, mica substrate, pulsed laser deposition

(Some figures may appear in colour only in the online journal)

1. Introduction

Flexible functional oxide heterostructures have become a hot topic in material science due to their outstanding characteristics including flexibility, portability, corrosion- and high-temperature resistance, etc. These superiorities make them attractive for being utilized in flexible electronic devices such as wearable devices, smart displays, sensors, aerospace field and so on [1–6]. Among these functional oxides, perovskite manganite oxides with a general formula $Ln_{1-x}A_xMnO_3$ (where Ln = La, Pr, Bi; A = Ba, Sr, Ca) have attracted intensive attention for both of condensed matter physics and practical device applications due to their various fantastic physical properties such as the colossal magnetoresistance, high degree of spin polarization, and the spontaneous charge-spin-orbital

* Authors to whom any correspondence should be addressed.

ordering [7–15]. In particular, $La_{0.7}Sr_{0.3}MnO_3$ (LSMO) has been widely studied because it has been considered as a promising material for spintronics due to the highest Curie temperature among the manganites ($T_C \sim 360$ K for bulk) and almost full spin polarization at the Fermi level, i.e. half metallicity. For this reason, the growth of high-quality of LSMO thin films has been attempted by various groups. Besides, a deep understanding of complicated competing interactions in LSMO, including the freedom of spin, charge, orbital and lattice, can further promote the control of its magneto-transport properties and engineer novel physical properties. On the other hand, LSMO can be regarded as pseudo-cubic perovskite structure with a lattice parameter of $a_c = 3.876$ Å, which is also widely utilized as an electrode for designing magnetoelectric and flexible electronic devices. Therefore, it can be seen that LSMO is an appropriate object to investigate the perovskite-mica van der Waals epitaxy heterostructures, no matter in the structural characterization or the application of spintronic devices [16–21]. Generally, the deposition of manganite oxides on flexible substrates is a forthright method to acquire flexible manganite heterostructures. To date, fluorophlogopite mica (mica) is widely utilized as flexible substrate due to its flexibility, transparency, and bargain price. The chemical formula of mica is $KMg_3(AlSi_3O_{10})F_2$ with lattice parameters of $a = 5.308$ Å, $b = 9.183$ Å and $c = 10.139$ Å, and bond angles of $\alpha = 90°$, $\beta = 100°$ and $\gamma = 90°$[4]. It is a kind of artificial metasilicate mica crystal that exhibits mechanical flexibility when it is been exfoliated to $10 \sim 50$ μm. Recently, many works have been devoted to fabricating epitaxial growth of flexible functional oxide thin films on mica substrates. For example, $Pr_{0.5}Ca_{0.5}MnO_3$ thin films were epitaxially grown on mica substrates with $SrTiO_3$ buffer layer showing an outstanding tunability of CMR ratio up to 1000% [4]. Huang *et al* reported that $La_{0.67}Sr_{0.33}MnO_3$/mica heterostructure exhibits an excellent ferromagnetic, magnetoresistance properties, and great flexible stability after mechanical bending [22]. However, transmission electron microscopy (TEM) images revealed that $La_{0.67}Sr_{0.33}MnO_3$ films show the mixture of (011) and (001) orientations.

Up to now, most of previous works related with epitaxial growth of perovskite-fluorophlogopite mica heterostructures have been focused on (111)-oriented films and buffer layers are highly needed for reducing the lattice mismatch and realizing the epitaxial growth. However, there are very few works reporting the direct growth of (100)-, (110)- or other oriented perovskite films without using buffer layers. In this work, we achieved the direct growth of epitaxial LSMO film on mica substrate without using buffer layer. Element interdiffusion was observed at the interface, hence, domain matching mode was proposed to understand the atomic relationship between the LSMO film and the mica substrate. It was found that, except for van der Waals interaction at the LSMO/mica interface, the interfacial energy aroused from chemical interaction also plays a pivotal role in realizing the direct growth of (110)-oriented LSMO film on mica substrate. Because of the in-plane multidomains with random rotation and the formation of oxygen vacancies, the ferromagnetism of the LSMO film is slightly reduced.

2. Experimental

Polycrystalline LSMO target was prepared by conventional solid-state sintering method. The detailed preparation procedures of LSMO target can be found in previous report [23]. Mica substrates were purchased from Changchun Taiyuan Co., China. The purity, optical transmittance, melting temperature, and resistivity of Mica substrates are round 99.99%, 90%, 1100 °C, and 10^{15} Ω cm^{-1}, respectively. Epitaxial LSMO films were grew on Mica (10 mm × 10 mm × 0.2 mm) substrates using pulsed laser deposition (PLD) by a KrF excimer laser ($\lambda = 248$ nm) with a fluence of 1.5 J cm^{-2} and a repetition rate of 2 Hz. During deposition, the substrate temperature was maintained at 700 °C and pure nitrogen (N_2) gas pressure was fixed at 0.1 mbar. After the growth, the LSMO films were annealed for 10 min and then cooled down to room temperature naturally.

The crystalline nature of the films was investigated by x-ray diffraction (XRD) on a high-resolution x-ray diffractometer (Panalytical Empyrean) using Cu K_α radiation ($\lambda =$ 1.5406 Å). This x-ray diffractometer was operated at 45 kV, 40 mA for all structural testing including θ-2θ scan, phi-scans and reciprocal space mapping. The θ-2θ pattern is ranged from 20° to 90°, which used step size of 0.01° and integration time of 60 s for every step. In reciprocal space mapping, a continue mode was applied in each 2θ scan with a step size of 0.02° and integration time of 60 s, and the step size of omega angle was 0.02°. As for phi-scans, ranged from 0° to 360°, the step size was 0.01° and integration time was 0.5 s. (TEM, Thermo Fisher Scientific TALOS F200X operated at 200 kV) was used to investigate the microstructure of the film, where the energy-dispersive spectroscopy (EDS) elemental mapping was utilized to investigate the element distribution including La, Mn and K. The surface morphology was investigated by atomic force microscopy (AFM, Asylum Research MFP-3D-SA). The surface morphology was investigated by (AFM, Asylum Research MFP-3D-SA). The AFM was working at AC tapping mode to acquire the surface topography of LSMO thin film. Non-conductive AC240TS-R3 Probe (Olympus Corporation) was selected as probe, which showed excellent results with a working frequency of around 70 kHz. Macroscopic magnetic measurements were performed by using a Quantum Design Physical Property Measurement System (PPMS). Temperature dependence of magnetization (M–T curve) was measured from 4 K to 300 K under a 500 Oe magnetic field applied along in-plane direction. Magnetic hysteresis (MH) loops were measured at several temperature points (5 K, 50 K, 150 K, 250 K and 275 K). For each loop, the magnetic field was ranged from −30 kOe to +30 kOe with a step size of 100 Oe.

3. Results and discussion

Figure 1(a) shows a typical XRD θ-2θ pattern of LSMO/mica heterostructure revealing that the LSMO film is single-phase. More importantly, apart from mica (00l) peaks, only pseudocubic-structure LSMO (110) and (220) peaks were

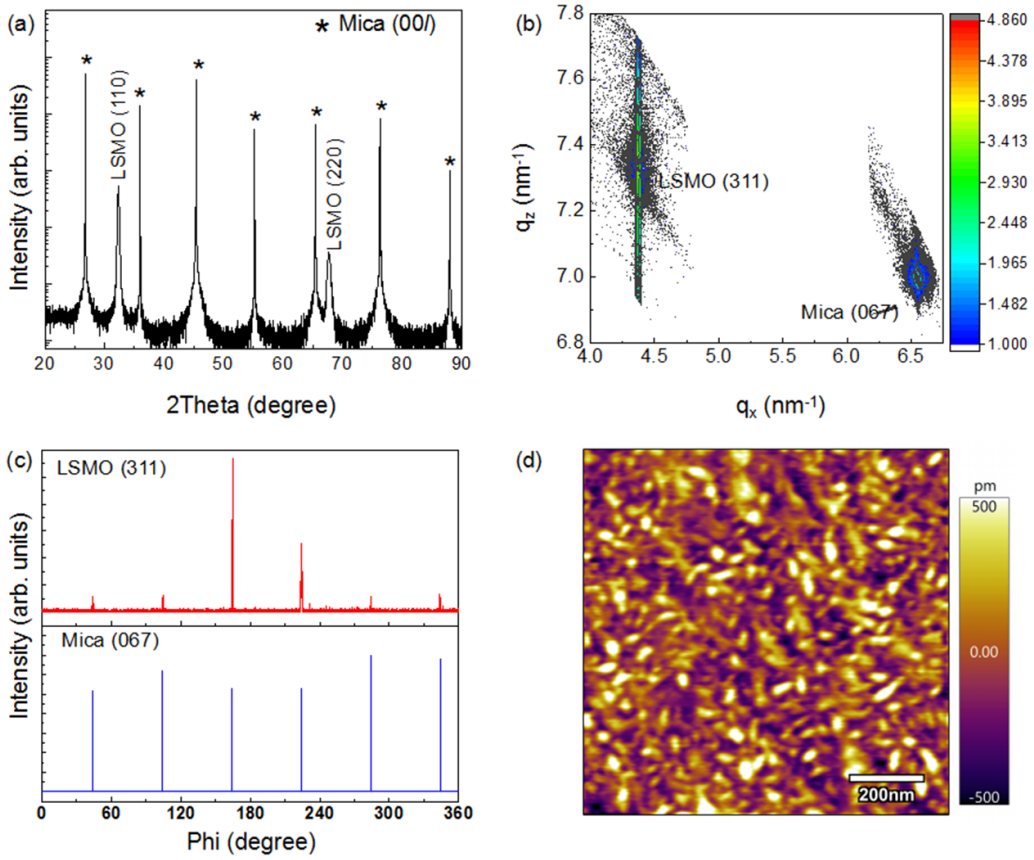

Figure 1. (a) A typical XRD θ-2θ pattern for LSMO/mica heterostructure. (b) Reciprocal space map of (311) and (067) bragg reflections of LSMO and mica, respectively. (c) ϕ–scans of LSMO (311) and mica (067). (d) A typical AFM height image (1×1 μm^2).

detected, indicating that there are no diffraction peaks from impurity or randomly oriented grains. Based on the LSMO peak position, the out-of-plane lattice parameter is calculated to be 1.364 Å, which is very close to the lattice parameter of the bulk (1.370 Å) [16]. It means that the strain induced by the lattice mismatch between the LSMO and mica substrate is almost relaxed. This is further validated by the x-ray reciprocal space map (RSM), as shown in figure 1(b). To further investigate the relationship of in-plane crystal orientations between the LSMO and mica substrate, phi-scans (ϕ–scans) were carried out on the skew planes of mica {067} planes ($2\theta = 95.1443°$, $\chi = 42.92°$) and LSMO {311} planes ($2\theta = 82.2069°$, $\chi = 30.54°$), respectively. As shown in figure 1(c), six sharp peaks for the LSMO {311} planes and mica {067} planes were observed. Theoretically, {311} planes of pseudocubic-perovskite LSMO are four-fold symmetry along [110] crystal orientation. {067} planes of C2/m-structure mica are four-fold symmetry along [00l] crystal orientation as well. The six-fold symmetry observed in ϕ–scans might be originated from the formation of in-plane multidomians [3]. Figure 1(d) showed the surface topography of LSMO/mica film. The observation of dozens-of-nanometers grains implies the formation of in-plane multidomains with random rotation. Well known, the ferromagnetism of manganite oxides originates from the double exchange effect that is a kind of long-range interaction. Here, the formation of in-plane multidomains with random rotation in LSMO/mica heterostructure may change the long-range interaction and in turn affect its magnetic properties. This will be discussed later. Besides, based on the results of RSM and ϕ–scans, the orientation relationship can be determined to be LSMO [110] ‖ mica [001] and LSMO [1-11] ‖ mica [060].

Figure 2(a) displayed the high-angle annular dark field TEM image of LSMO/mica heterostructure viewed along the zone axis of LSMO [002]. To examine the element distribution, EDS elemental mapping of La, Mn and K was performed and shown in figures 2(b)–(d). It can be seen that La, Mn elements are uniformly distributed in the LSMO film. In addition, element inter-diffusion between the LSMO film and mica substrate was also identified at the interface. This strongly indicates that surface or interfacial atomic structure of mica is changed with K^+ ions diffusion. Hence, sectional Al^{3+}/Si^{4+} ions may be exposed and formed bonds with LSMO at the interface. The microstructure of the LSMO was further investigated by scanning transmission electron microscopy, as shown in figure 2(e), revealing the high quality of LSMO film. The SAED patterns (figure 2(f)) further confirm that the growth orientations of LSMO are along (110) and (220). This is consistent with the observation of XRD result.

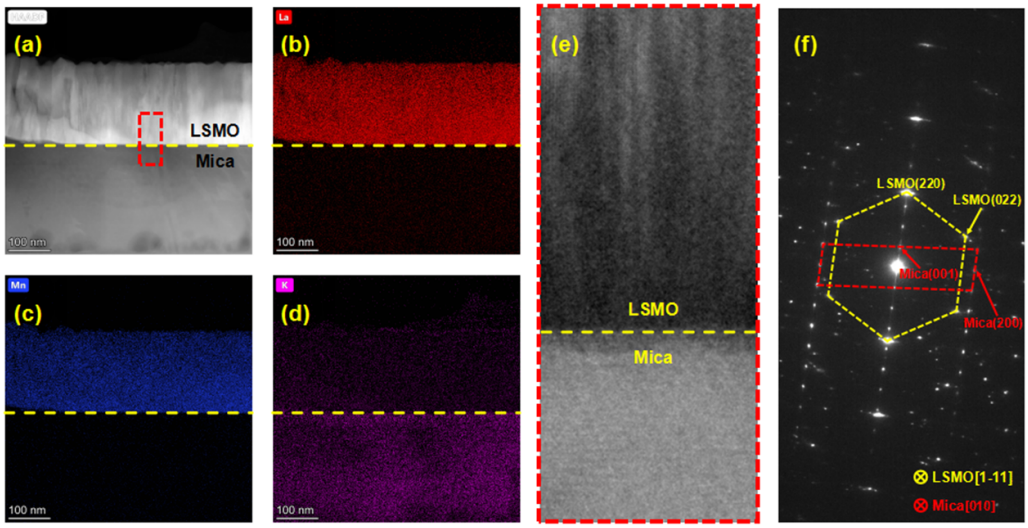

Figure 2. (a) Cross-section STEM image of LSMO/mica heterostructure. EDS elemental mapping of (b) La, (c) Mn and (d) K. (e) High-resolution STEM image of interface corresponding to the rectangle region in (a). (f) Selected area electron diffraction (SAED) patterns acquired from LSMO film and mica substrate.

In conventional epitaxial heterostructure engineering, the lattice matching epitaxy (LME) theory was successful in describing the epitaxial behaviour of film and substrate with similar crystal symmetry and small misfit of less than 7%–8%. However, the large misfit systems were unable to be explained by LME. Around beginning of 21th century, J. Narayan *et al* present a unified model called domain matching epitaxy (DME) to depict the stacking mode of epitaxial thin film on single crystal substrate, even though a huge misfit was exists between the epitaxial layer and substrate. Some atomic-level details in different systems were demonstrated to illustrate this concept, for example, TiN/Si (100) with 3/4 matching, AlN/Si (100) with 4/5 matching and ZnO/α-Al_2O_3(0001) with 6/7 matching across the film-substrate interface [24].

Due to the epitaxial growth of LSMO film on mica substrate with multi-domain and element inter-diffusion between the LSMO film and mica substrate at the interface, some specific atomic combine mode or alignment pattern between the LSMO film and mica substrate may be formed. Based on above results, we put forward a conjecture on how the LSMO film is epitaxial grew on mica substrate according to the DME theory [25].

In order to sketch the atomic relationship, we used Visualization for Electronic and STructural Analysis (VESTA) software to describe the crystal structure of the LSMO film and mica substrate, as shown in figure 3. Chromatic spheres and dash lines were used to represent the respective structures and unit cells of the LSMO film and mica substrate. Cartesian coordinates are labelled to identify the lattice orientation.

The La^{3+}/Sr^{2+} ions are combined by La/Sr-O bonds, arranging on the LSMO {110} planes in the rectangle array with a side length of 5.48 Å and 3.87 Å, respectively. For the mica substrate, the K^+ ions arrange on the fresh peeled surface of mica (00l) planes in the parallelogram array with a side length of 5.30 Å. Considering the element inter-diffusion at the interface, the Al^{3+}/Si^{4+} ions of mica arrange on the mica (00l) planes in the regular hexagon array with a side length of 3.07 Å, which may be exposed and formed bonds with LSMO{110} planes. Two stack modes were further brought up to describe the combine pattern of unit cells between the LSMO film and mica substrate. The first mode is depicted as figure 3(a) to explain the situation that K^+ ions are perfectly arranged on the surface of mica substrate in a parallelogram array. This is a common mode of van der Waals epitaxy. However, as evidenced by EDS mappings (figures 2(b)–(d)), element inter-diffusion happened at the interface between the LSMO film and mica substrate. As a consequence, surface atoms of mica are possibly changed with the diffusing of K^+ ions. Based on the chemical bonds of mica substrate, we speculate that sectional Al^{3+}/Si^{4+} ions may be exposed and formed bonds with La/Sr-O at the interface, as shown in figure 3(b). Similar element inter-diffusion was reported in the interface of CdTe/mica heterostructure. By using the first-principle calculations, Sun *et al* uncovered that van der Waals interaction and interfacial chemical interaction contribute 20% and 80% of the total interfacial energy, respectively [26]. Therefore, except for van der Waals interaction at the LSMO/mica interface, a large contribution of the interfacial energy due to chemical interaction may play a pivotal role in achieving the direct growth of (110)-oriented LSMO film on mica substrate.

As we have mentioned earlier, a multi-domain structure may exist in LSMO. In order to further investigate the relationship between multi-domain LSMO and mica, a top-view of atom arrangement was depicted and discussed to reveal their epitaxy relationship between LSMO thin film and mica substrate as shown in following figures 3(c) and (d). Before our discussion, the mismatch ε utilized in this work was defined as:

$$\varepsilon = (d_{\mathrm{LSMO}} - d_{\mathrm{mica}})/d_{\mathrm{mica}} \times 100\%$$

as usual. According to the DME theory, the matching of integral multiples of lattice planes leads to a residual mismatch

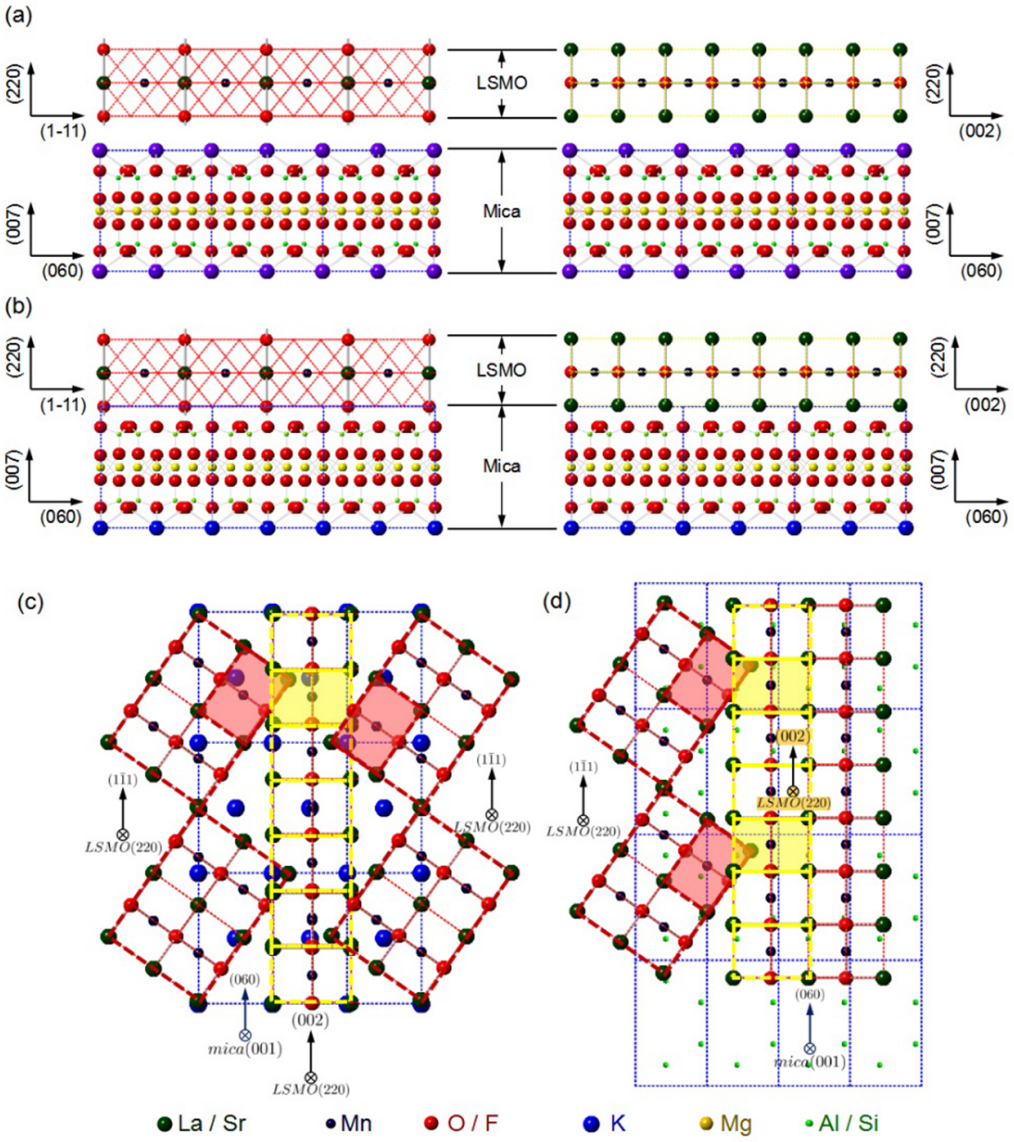

Figure 3. Side views of lattice relationship between LSMO film and mica substrate depicted in (a) van der Waals mode and (b) bonding mode. Top views of lattice relationship between LSMO film and mica substrate in (c) van der Waals mode and (d) bonding mode, respectively. Where, the blue rectangles mark the mica, while red and yellow present LSMO (1-11) and LSMO (002) domains, respectively. Graphic examples of different atoms are listed below.

$$\varepsilon_r = (m \times d_{\mathrm{LSMO}} - n \times d_{\mathrm{mica}}) / (n \times d_{\mathrm{mica}}) \times 100\%$$

where, the d_{LSMO}, d_{mica} were interplanar crystal spacings of LSMO and mica, while m, n were positive integer.

The epitaxial relationship between (110)-LSMO and mica substrate was determined as (220) LSMO (1-11) ∥ (001) mica (060) by XRD. It is easy to acquire the lattice spacing of every lattice plane, for example, $d_{\mathrm{LSMO}(1-11)} = 2.238\,\text{Å}$, $d_{\mathrm{LSMO}(002)} = 1.938\,\text{Å}$ and $d_{\mathrm{mica}(060)} = 1.5305\,\text{Å}$. Hence, the mismatch between the film and substrate were

$$\varepsilon_{\mathrm{LSMO}(1-11)-\mathrm{mica}(060)} = +46.2\%$$

and

$$\varepsilon_{\mathrm{LSMO}(002)-\mathrm{mica}(060)} = +26.6\%,$$

respectively. The thin film was unable to achieve a perfect epitaxial growth on substrate under such large lattice mismatch. Here, two domain matching models was analysed in detail. In the first mode, noted as van der Waals mode, the K^+ ions were perfect arranged on the surface of mica as shown in figure 3(c), a 12/18(i.e. 2/3) matching along LSMO [1-11] direction could release the residual mismatch low to

$$\varepsilon_r = \frac{12 \times d_{\mathrm{LSMO}(1-11)} - 18 \times d_{\mathrm{mica}(060)}}{18 \times d_{\mathrm{mica}(060)}} \times 100\% = -2.5\%.$$

As for LSMO (002) plane, the residual mismatch between LSMO (002) and mica (060) was only

$$\varepsilon_r = \frac{14 \times d_{\mathrm{LSMO}(002)} - 18 \times d_{\mathrm{mica}(060)}}{18 \times d_{\mathrm{mica}(060)}} \times 100\% = -1.5\%$$

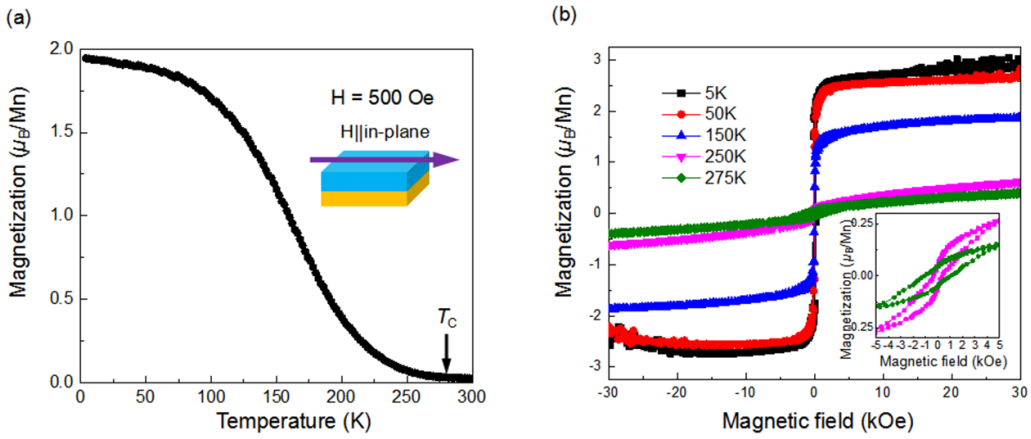

Figure 4. (a) Temperature dependence of magnetization (*M–T* curve) of LSMO/mica film measured under a 500 Oe magnetic field applied along in-plane. (b) Magnetic hysteresis loops of LSMO/mica film measured at temperatures of 5 K, 50 K, 150 K, 250 K and 275 K, respectively. The insets are zoom-in view of magnetic hysteresis loops of 250 K and 275 K.

with a 14/18 (i.e. 7/9) domain matching structure. In another mode, called bonding mode, as shown in figure 3(d), the Al^{3+}/Si^{4+} ions may exposing due to the diffusion of K^+ ions, and bonding with LSMO. Similarly, the LSMO kept the same domain matching number to that of van der Waals mode to reduce the lattice mismatch, that was

$$12 \times \mathrm{LSMO}\,(1-11) \parallel 18 \times \mathrm{mica}\,(060)$$

and

$$14 \times \mathrm{LSMO}\,(002) \parallel 18 \times \mathrm{mica}\,(060)\,.$$

The temperature dependence of magnetization (*M–T* curve) obtained by field-cooling under 500 Oe, applied parallel to the *x–y* plane of LSMO, was shown in figure 4(a). Ferromagnetic behaviour with a T_C of 280 K was observed for the LSMO film. The value of T_C observed in the LSMO/mica heterostructure is lower than that of (110) LSMO films grown on rigid substrates [27–31] and LSMO bulks [23, 32]. MH loops (magnetization vs the magnetic field, *M–H*) were also measured along the *x–y* plane of LSMO at the temperatures of 5 K, 50 K, 150 K, 250 K and 275 K (figure 4(b)). We can see that the magnetization decreases with the increase of the measured temperature. However, as shown in the inset of figure 4(b), the MH loops of 250 K and 275 K show an obvious hysteresis phenomena, indicating the ferromagnetism of LSMO/mica heterostructure still exists near T_C. Besides, saturation magnetic moment (M_S) given by the *M–H* loop measured at 5 K is around 3.04 μB Mn^{-1}, which is slightly lower than that of (110) LSMO films grown on rigid substrates (3.14μ_B Mn^{-1}) [29]. Well known, double exchange (DE) interaction is responsible for ferromagnetism in perovskite manganite, presented by Zener as early as 1951 [33], which is a kind of long-range interactions. As discussed in the AFM image shown in figure 1(d), dozens-of-nanometers grains were observed, implying the formation of in-plane multidomains with random rotation. We also found that the crystallinity of the LSMO film grown on mica substrate was inferior to that of the LSMO films grown on rigid substrate. Consequently, the long-range DE interaction is strongly affected by the uncomplete crystallization of LSMO grains, resulting in the degeneration of saturation magnetic moment. On the other hand, the energy level of Mn 3d-orbit electrons split under the impact of crystal-field, low-energy itinerant e_g electrons hopping along the Mn^{3+}–O^{2-}–Mn^{4+} chains. Here, during the deposition, pure nitrogen gas was used to grow (110)-oriented LSMO film on mica substrate. In turn, it can be expected that oxygen vacancies were formed in the LSMO film. This may further influence the hopping of e.g. electrons, which finally induces the degeneration of saturation magnetic moment as well [34].

4. Summary

In conclusion, by using the PLD method, (110)-oriented LSMO film was directly fabricated on mica substrate. Owing to the element inter-diffusion at the LSMO/mica interface, domain matching relationship between the LSMO film and mica substrate are proposed by VESTA software and discussed. We found that, except for van der Waals interaction at the LSMO/mica interface, a large contribution of the interfacial energy caused by chemical interaction plays a pivotal role in achieving the direct epitaxial growth of (110)-oriented LSMO film on mica substrate. Considering the element inter-diffusion at the interface and the formation of oxygen vacancies in the LSMO film, the saturation magnetic moment and ferromagnetic T_C of the LSMO film were reduced. Our work provides a new pathway to directly fabricate (110) perovskite functional oxide films on flexible mica substrates and also opens a new door to construct the flexible electronic devices by using different oriented functional oxide films.

Data availability statement

All data that support the findings of this study are included within the article (and any supplementary files).

Acknowledgments

H Y acknowledges support from the National Natural Science Foundation of China (Grant Nos. 11774172, 5217020745, and 9216310165). W-W L acknowledges support from the National Natural Science Foundation of China (Grant No. 52102177), the National Natural Science Foundation of Jiangsu Province (Grant No. BK20210313), and the Jiangsu Specially-Appointed Professor Program. H Y and W-W L also acknowledge support from the Top-notch Academic Programs Project of Jiangsu Higher Education Institutions (TAPP). S X and R T acknowledge support from the National Natural Science Foundation of China (Grant No. 51772200). D Z, J L and H W acknowledge the support from the US National Science Foundation for the TEM work at Purdue University (DMR-1809520 and DMR2016453).

ORCID iDs

Jiyu Fan https://orcid.org/0000-0001-6698-6384
Rujun Tang https://orcid.org/0000-0001-6335-2095
Haiyan Wang https://orcid.org/0000-0002-7397-1209
Haizhong Guo https://orcid.org/0000-0002-6128-4225
Weiwei Li https://orcid.org/0000-0001-5781-5401

References

[1] Miao J *et al* 2017 *ACS Nano* **11** 6048–56
[2] Cai S *et al* 2019 *Adv. Mater.* **31** 1808138
[3] Xu R *et al* 2020 *ACS Appl. Mater. Interfaces* **12** 16462–8
[4] Yen M *et al* 2020 *Adv. Funct. Mater.* **30** 2004597
[5] Zhang X *et al* 2021 *Ceram. Int.* **47** 13156–63
[6] Zhang X *et al* 2021 *ACS Appl. Mater. Interfaces* **13** 47764–72
[7] Jin S *et al* 1994 *Science* **264** 413–5
[8] Asamitsu A *et al* 1997 *Nature* **388** 50–52
[9] Xiang P-H *et al* 2011 *Adv. Mater.* **23** 5822–7
[10] Fan J *et al* 2019 *J. Alloys Compd.* **806** 753–60
[11] Li W *et al* 2020 *Mater. Horiz.* **7** 2832–59
[12] Li W *et al* 2020 *Adv. Sci.* **7** 1901606
[13] Li W *et al* 2020 *Adv. Funct. Mater.* **30** 2001984
[14] Chen S *et al* 2021 *Sci. China Phys. Mech. Astron.* **64** 287711
[15] Huang J *et al* 2021 *MRS Bul.* **46** 159–67
[16] Thiele C *et al* 2007 *Phys. Rev.* B **75** 054408
[17] Hernandez-Martin D *et al* 2020 *Phys. Rev. Lett.* **125** 266802
[18] Perna P *et al* 2017 *Adv. Funct. Mater.* **27** 1700664
[19] Zhang S *et al* 2017 *Adv. Mater.* **29** 1703543
[20] Zhu M *et al* 2017 *Adv. Funct. Mater.* **27** 1605598
[21] Spurgeon S R *et al* 2014 *Acs Nano* **8** 894–903
[22] Huang J *et al* 2018 *ACS Appl. Mater. Interfaces* **10** 42698–705
[23] Fan J *et al* 2015 *J. Mater. Sci.* **50** 2130–7
[24] Narayan J and Larson B C 2003 *J. Appl. Phys.* **93** 278–85
[25] Zhang K H L *et al* 2012 *Cryst. Growth Des.* **12** 1000–7
[26] Mohanty D *et al* 2018 *Phys. Rev. Mater.* **2** 113402
[27] Köster S A *et al* 2002 *Appl. Phys. Lett.* **81** 1648–50
[28] Majumdar S *et al* 2013 *J. Phys.: Condens. Matter* **25** 376003
[29] Chen S *et al* 2018 *Ceram. Int.* **44** 13695–8
[30] Wenhao Y *et al* 2015 *J. Appl. Phys.* **117** 17E102
[31] Quan Z *et al* 2017 *Appl. Phys. Lett.* **110** 072405
[32] Gaur A and Varma G D 2006 *J. Phys.: Condens. Matter* **18** 8837–46
[33] Zener C 1951 *Phys. Rev.* **81** 440–4
[34] Guo H *et al* 2016 *Adv. Mater. Interfaces* **3** 1500753